

# SENSITIVITY FACTOR ANALYSIS AND OPTIMIZATION OF RECYCLED GLASS FIBRE COMPOSITE WASTE REINFORCED FE-RICH INORGANIC POLYMER

Zhang Y<sup>1,2,\*</sup>, Pontikes Y<sup>1</sup>, van Vuure A<sup>1</sup>, Lessard L<sup>2</sup>,

<sup>1</sup> Department of Materials Engineering, KU Leuven, Heverlee, Belgium

<sup>2</sup> Department of Mechanical Engineering, McGill University, Montreal, Canada

\* Corresponding author (yixue.zhang@mail.mcgill.ca)

**Keywords:** *Glass fibre thermoset waste, Mechanical recycling, Inorganic polymer*

## ABSTRACT

This work develops an optimized recycling route that provides a solution for two kinds of residues. Mechanically recycled glass fibre reinforced composite (GFRP) waste (including all resin residues) was coldly incorporated into a sustainable Fe-rich inorganic polymer (IP), a by-product of the non-ferrous metal industry, to produce sustainable reinforced cementitious material. The optimization of the proposed recycling route has been studied herein. Different mechanical techniques to improve the efficiency of the grinding process and retain fibre length have been investigated. Sensitivity factor analysis on the mechanical performance of the final products was conducted by using a Taguchi design method and ANOVA, and a proposed reasonable optimization was suggested. The measured compressive strength for the optimized material reached 101 MPa, and the optimized flexural strength amounted to 28 MPa at 7 days of curing. The flexural strength enhancement compared to the state-of-the-art stands out, reaching a gain of 215%; the improvement in compressive strength is at a more moderate level of about 32%. The effectiveness of the properties of the optimum composites compared to the literature shows the success of the optimization actions for the recycling route used in this work.

## 1 INTRODUCTION

The world needs a low carbon revolution, and processes to recycle end-of-life (EoL) glass fibre reinforced polymer (GFRP) with a thermoset matrix are integral to sustainable development. Due to the characteristics of GFRP recycling, such as the non-remoulding nature of thermoset resins, the low price of virgin fibres (2€/kg), low calorific value and high left-over burnt ash content, mechanical recycling shows more promise in practice [1]. However, some attempts to commercialize grinding GFRP to fine material for use as filler or reinforcement as a recycling route have failed (e.g., Phoenix Fibreglass [2], ERCOM GmbH [3]). Reasons behind this are mainly attributed to the high energy input required to crush the material finely, a lack of cost-effective end-use applications for the recyclates, and limited ongoing sales in the market (lack of economies of scale).

To increase the market readiness of GFRP recyclates, innovative, sustainable and economical mechanical recycling techniques as well as new application possibilities for recycling need to be identified. The present research team proposed a promising recycling route and verified the high potential to cold incorporate mechanically recycled GFRP waste into a novel Fe-rich inorganic polymer (IP) [4]. The Fe-rich IP used was a by-product of non-ferrous metal production via pyrometallurgical techniques. Fire resistance, comparable mechanical strength, fast curing time, (acidic or sulphate) chemical resistance and 17%-47% lower CO<sub>2</sub> emissions of production are some of the enhanced properties of IPs compared to ordinary Portland cement (OPC) [5–7]. However, the hardened IP shows brittleness

and suffers from low tensile strength. GFRP waste in IP can be envisaged as an end-user application for recyclates, overcoming the limitations of the inorganic polymers.

Insufficient research has been carried out so far on the parameter sensitivity analysis of recycled GFRP reinforced inorganic polymer (rGF-IP). According to the authors, the available data are restricted in three ways. First, the Fe-rich inorganic polymer in this paper is a novel secondary product of non-ferrous metal industries; many of its properties have not been studied widely. Its high iron content (48.7 wt%) leads to forming a 3D Fe<sup>3+</sup>-aluminosilicate network with Fe<sup>2+</sup> arranged in layers with a trioctahedral configuration after polycondense [7]. Such cross-linked networks contribute to different fresh/hardened matrix properties compared with OPC or commonly-used geopolymers, such as metakaolin and fly ash. Secondly, past studies mainly focus on incorporating pure/virgin glass fibres in cement, with little use of various GFRP waste (fibre, powder, mixture and scrap) simultaneously. These wastes generally have more complex characteristics, such as multiple length distribution, fluffiness, and irregular resin residues attached to the fibres. The type of reinforcers, fibre content, orientation and distribution, brittleness, the pore structure of the cementitious matrix and fibre-matrix interaction all matter in the final performance. Lastly, previous studies mainly obtained results with a particular production method, and those studies did not explore the effects of different mixing technologies on the composites [4,8]. Parameters such as mixing technologies, sequence, time, speed and temperature can alter the paste's entrapped air and fibre dispersion [9].

From the previous analysis, grasping the effects of the different combinations of the materials' characteristics on the mechanical properties of rGF-IP is necessary for optimizing the proposed recycling route. However, many factors affect the rGF-geopolymer and sometimes interact, and the relationship between various factors is complex and difficult to determine through the results of experiments. Therefore, a sensitivity factor analysis of the mechanical properties of rGF-IP through experiments is necessary. The first step in this study is to explore different mechanical techniques to improve the efficiency of the grinding process and retain fibre length. In the second stage, the Taguchi method was used to design experiments and, together with Analysis of Variance (ANOVA), to explore the significance of various factors on the final composites' properties. Effects of three parameters, including the fibre aspect ratio, fibre content and the producing method, on the flexural/compressive strength, Young's modulus, porosity distribution, and fibre orientation of the rGF-IP were analyzed, and a reasonable optimization suggestion was proposed.

## 2 MATERIALS AND METHODOLOGY

### 2.1 Materials

The Fe-rich inorganic polymer (IP) used in this study originates from a secondary non-ferrous metallurgical process. It was milled to a suitable fineness level—approximately 4000 cm<sup>2</sup>/g and mainly consisted of 48.7 wt.% iron and 25.5 wt.% silica with moderate amounts of aluminum (7.74 wt.%), calcium (2.91 wt.%), and magnesium (1.22 wt.%) oxides. An activating solution (SiO<sub>2</sub>/K<sub>2</sub>O = 2 and H<sub>2</sub>O/K<sub>2</sub>O = 20, by molar ratio ) from the previous study [4] was employed in this study. The GFRP waste samples were acquired from in-house produced GFRP flat panels manufactured by vacuum infusion with epoxy resin and E-glass fabric (52wt.%).

### 2.2 Mechanical recycling optimization

Following the results of the previous study [4], the optimization of mechanical recycling aims to extract a high percentage of fibre concentrate compared to the mixture of fillers. Herein, two mechanical grinding techniques, disk and roller milling, were used, and their efficiencies in recovering the slender glass fibres were compared.

Figure 1 (1) depicts the mechanical recycling processes for GFRP waste. A guillotine shear first shredded the GFRP waste panels to reduce their size and convert them to suitable feeding materials for the milling equipment. The grinding machine used in route 1 was a disc mill that relies on the disc's friction and the ring on the particles inside the jar to mill the material. The rolling milling device utilized in route 2 was a Wellman mill that uses the process of stress and attrition to reduce the structural shapes when passing through the gap between rollers. Herein, this device was roughly crushing the composites (medium-hard). Afterwards, the milled GFRP strips (in route 2) were further dispersed to fibres via a Hobart mixer (wet mixing). The obtained recyclates (in both routes) are complex mixtures with diverse grade sizes. They were separated into fine powders, fibrous grades, and large fibre bundles using multiple staged sieves with varying mesh sizes. The route yielding more slender fibres is considered the optimized recycling route, and the GFRP recyclates obtained by that route will be utilized to make rGF-IP samples.

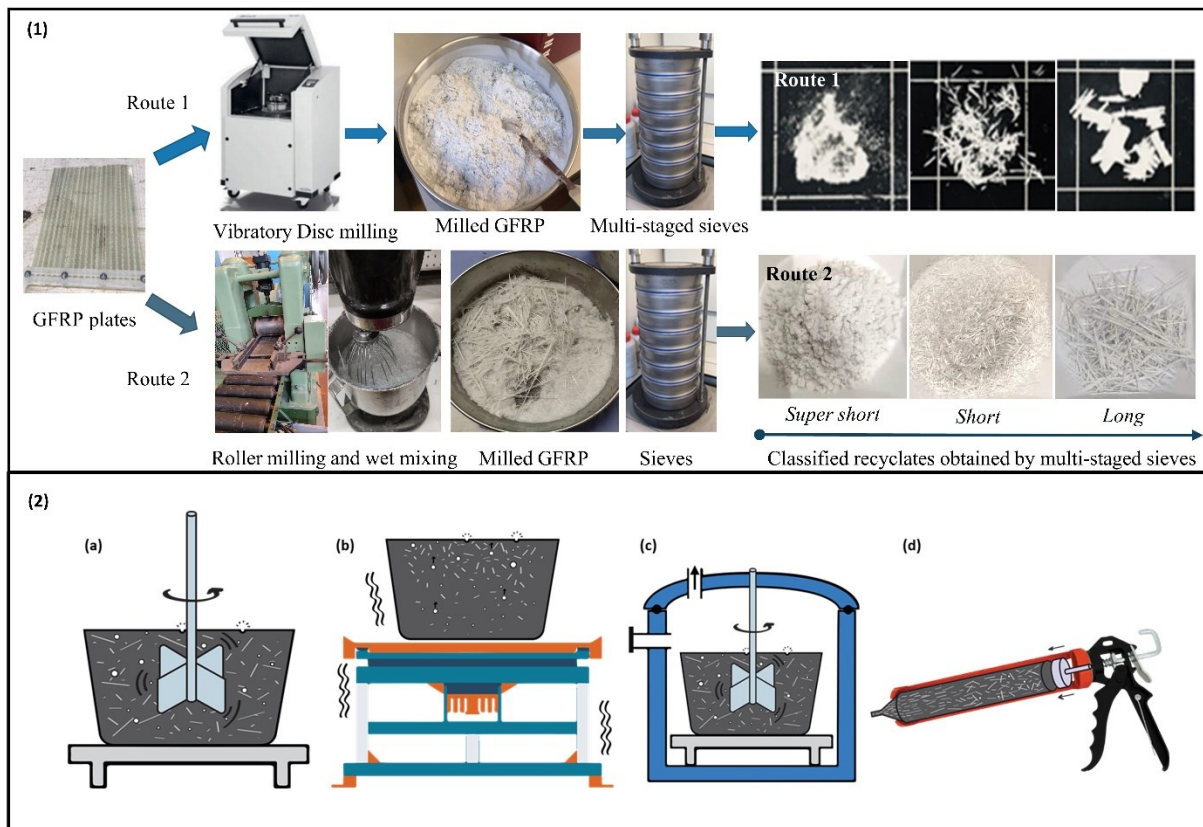


Figure 1. (1) Mechanical shredding and milling processes of the GFRP waste; (2) four different mixing technologies.

### 2.3 Taguchi orthogonal design

Factor sensitivity analysis was achieved by using the Taguchi orthogonal method with three parameters and four levels (Table 1). The producing method (Pm), rGFs aspect ratio (Ar), and fibre content (Fn) were selected as controllable affecting parameters. Settings of parameters were determined by the  $L_{16}$  ( $4^3$ ) orthogonal array with four levels and four specimens for each combination, giving 64 specimens in total (Table 2).

The sequence for making rGF-IP composites was: (1) mixing the dried IP powder with an alkaline activator manually (~1 min) into a wet paste; (2) gradually mixing the GFRP recycled material with the wet paste. In step (2), mixtures of different recyclates and contents underwent different mixing technologies: regular mixing (M), vibrating mixing (Vib), vacuum mixing (Vm), and vacuum mixing with a cartridge to squeeze the paste out into the mould (VmC)

(illustrated in Figure 1 (2)). To eliminate the influence of mixing energy, the mixing time was set to 5min. Afterwards, the mixture was directly poured into the plastic mould. For samples made by Vib, a vibrator was used after mixing; the mixture was placed on a shaker table and vibrated for 5min at a medium speed to release the entrapped air before casting. In the case of Vm, within 10s after the starting of mixing, a reduction from ambient pressure to 100 mbar was established by a vacuum pump, and the 100 mbar was kept until the end of the mixing procedure. In terms of VmC, the smooth mixture was placed in a cartridge and was squeezed out into the mould (2cm\*2cm\*8cm). All samples were cured under controlled conditions (20±2°C and relative humidity not less than 50%) for 24h for demoulding and left to cure until the satisfactory total curing time (7 days).

Table 1. Experimental range and levels of variables

Control variables	Symbol	Unit	Levels			
			1	2	3	4
Producing method	<i>Pm</i>	-	M	Vib	Vm	VmC
rGFs aspect ratio	<i>Ar</i>	mm/mm	N/A	SS	S	L
rGFs content	<i>Fn</i>	vol%	0.5	1.5	3.5	6

M: Regular mixing Vib: Vibrating mixing Vm: Vacuum Mixing VmC: Vacuum mixing and cartridge.

In the second stage, experiments were performed. Response values, porosity (P) in the matrix, fibre orientation distribution ( $\alpha$ ), flexural strength (Fs), compressive strength (Cs), and flexural Young's modulus (Es), were obtained. Minitab 19 was used for analyzing the experimental results. Ranking of selected parameters in terms of contribution to response values was done via analyzing signal-to-noise ratios (S/N) and analysis of variance (ANOVA). Here, "signal" implies the (wanted) mean value while "noise" represents the (unwanted) standard deviation term [10]. A Higher S/N ratio means that lower variability in the process is ensured by maximizing the response.

#### 2.4 Testing methods

Effects of fibre orientation are considered by using a so-called orientation factor  $\alpha$ , a ratio of the number of fibres counted in a specific cross-sectional area over its theoretical number, obtained by (1) [11]:

$$\alpha = \frac{n}{th} = n \frac{A_f}{V_f A} \quad (1)$$

Where  $n$  is the number of observed fibres,  $th$  is the theoretically expected number of fibres,  $A_f$  is the average cross-sectional area of the observed fibres,  $V_f$  is the fibre volume fraction, and  $A$  is the total cross-sectional area of the composite.

The value of the orientation factor  $\alpha$  represents how freely the fibre can rotate in all directions in the bulk zone. The lower the overall orientation factor, the higher the isotropy of the analyzed cross-sectional surface. For example, a value of 0.5 represents a 3D isotropic condition where fibres could rotate freely in all directions; a higher value of around 0.8 is generally observed for a 2D anisotropic condition where fibres tend to be aligned [12]. The calculation of the orientation factor  $\alpha$  is challenging. The difficulty lies in the measurement of  $n$  and  $A_f$ , as individual fibres (~15  $\mu$ m in diameter) in the IP matrix cannot be easily identified by visual inspection. Besides, the irregularity and varying cross-section of recycled fibres hinder the measurement of  $A_f$ . An easy recycled fibre counting method that can automatically and spatially detect fibres was developed by micro-computed tomography ( $\mu$ -CT) (Figure 2). To carefully track the single fibres, the spatial resolution of  $\mu$ -CT was limited to 5.75  $\mu$ m by multi- $\mu$ -CT scanning volume reduced samples (6mm\*6mm\*20mm, by carefully sawing the original IP block into three subparts) at 110kV and 110  $\mu$  with a 1mm Cu-filter. The scanned images were then reconstructed with Phoenix Datos|x - CT Data acquisition software and analyzed by Avizo software (Thermo Fisher).

The porosities for hardened reinforced samples were measured before the mechanical test by  $\mu$ -CT and mercury intrusion porosimetry (MIP).  $\mu$ -CT was used to detect macro air voids ( $>200\mu\text{m}$ ); MIP was used to analyze capillary pores and micropores ( $4\text{nm}-200\mu\text{m}$ ). Their sum up is the total porosity of the sample.

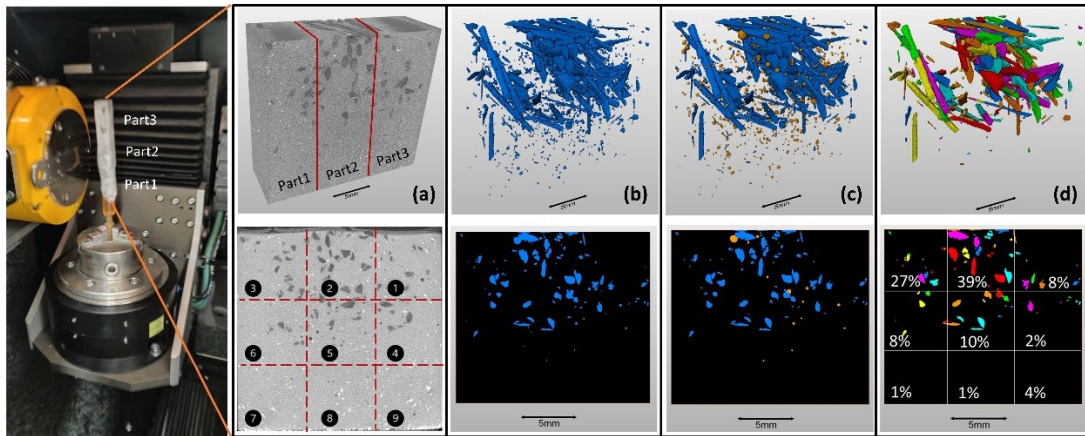


Figure 2. (a) IP block was sawn into three parts and scanned; the scanned images were "sectioned" into nine equal squares for fibre measurements; (b) a dual-threshold binarisation removed IP grains; (c) pores were further removed by sieving out sphere-like objects; (d) the remaining recycled fibres were separated, and numbers ( $n$ ) and cross-sectional areas ( $A_f$ ) were measured.

The mechanical tests of rGFs-IP composite samples ( $2\text{cm} \times 2\text{cm} \times 8\text{cm}$ ) cured for 7 days were performed at room temperature using an Instron 5985 mechanical testing machine according to European standard EN 196-1:2005 [13]. In the bending case, the 3D digital image correlation (3D DIC) determined the strain fields of rGFs-IP samples. The slope of the stress-strain curve at the initial linear stage was measured as Young's modulus.

### 3 RESULTS AND DISCUSSION

#### 3.1 Optimization of the recycling process and rGFs characteristics

From a visual inspection of the resulting samples, the disc milling system tends to reduce fibre length excessively and produces GFRP recyclates with a maximum fibre length of around 2-5mm and an aspect ratio of 5-6, giving rise to an intertwined mixed flurry of glass fibres with parts of the polymer (Figure 1). The roller milling produces more concentrated slender glass fibres; its content is highly dependent on the setting parameters of the roll gap and mixing time. After evaluating various set-ups, it was concluded that the highest fraction of slender glass fibres is obtained when the gap between rollers is approximately  $1/3-1/2$  of the thickness of the feed GFRP panels. The optimum milling route for mechanical processing of in-house GFRP waste is (1) primary shredding of GFRP into a slender shape; (2) milling of the shredded material via roller milling with medium speed, roller gap set to  $1/3$  of the thickness of feed material; (3) mixing the crushed material with medium speed for 10-15mins with water in the mixing container; and (4) drying the milled GFRP waste (a mixture of fibres and powders) at  $50^\circ\text{C}$  for 24h, then sieving by multiple staged sieves with decreasing varying mesh sizes from top to bottom.

Physical features suggest that recycled GFRP waste fractions from roller milling can be roughly divided into three categories: super short (SS) fibre fluff, short (S) fibres and long (L) fibre bundles. The fluffy recyclate and short fibres only represent 10 wt.% and 11 wt.% of the total waste, respectively. L fibre bundles were numerically dominant, accounting for 79 wt.% of the total recyclate. This large number indicates the efficiency and benefit of using roller milling. The mean fibre length for the combined recyclates was approximately 13mm, while the corresponding individual mean sizes for SS, S, and L were 0.68mm, 7.3mm and 32mm, respectively. The corresponding average

aspect ratios have dramatically increased from 3 via 13 to 25, almost five times the maximum aspect ratio of the fibres recycled from disc milling. Interestingly, fibrous particles (L and S) generally contained more resin residues than ultra-short fractions (SS), indicating that roller milling is a relatively mild grinding process. The majority of cured epoxy residues were in the form of a shell partially covering the recycled glass fibres rather than ground particles.

**3.2 Sensitivity factor analysis on rGFs-IP performance characteristics**

The S/N ratio and factor contributions of selected parameters to rGFs-IP performance are summarized in Figure 3. The experimental results are concluded in Table 2.

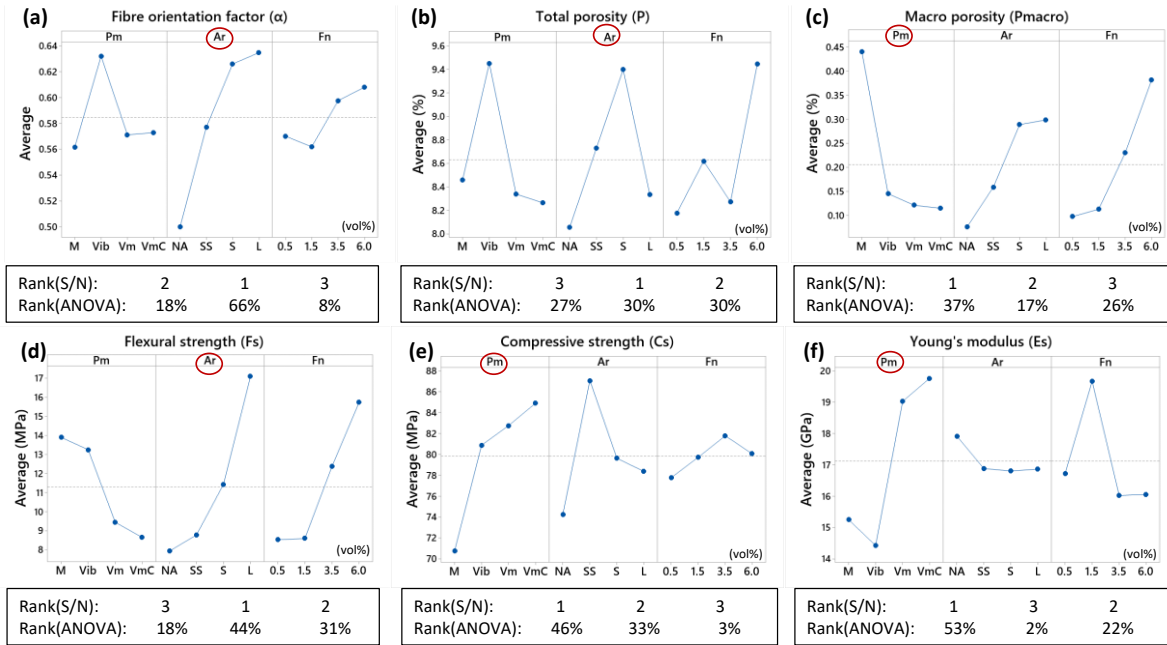


Figure 3. Effects of selected parameters on the rGFs-IP performances.

Table 2. L<sub>16</sub> orthogonal mixture designs and experimental results.

Index	Pm	Ar	Fn (vol%)	$\alpha$	P(%)	$P_{macro}$ (%)	$F_s$ (MPa)	$C_s$ (MPa)	$E_s$ (GPa)
1	M	NA	0.5	0.50	7.56	0.12	8.47	65.85	14.23
2	M	SS	1.5	0.53	8.42	0.14	7.44	77.88	19.52
3	M	S	3.5	0.59	8.49	0.61	12.95	70.74	12.68
4	M	L	6	0.63	9.37	0.89	26.71	68.64	14.62
5	Vib	NA	1.5	0.50	8.64	0.05	7.10	77.75	16.36
6	Vib	SS	0.5	0.60	9.33	0.11	8.46	80.81	14.72
7	Vib	S	6	0.73	11.50	0.29	17.17	83.98	11.40
8	Vib	L	3.5	0.70	8.34	0.13	20.26	80.98	15.25
9	Vm	NA	3.5	0.50	7.94	0.06	7.15	74.26	19.75
10	Vm	SS	6	0.58	8.84	0.27	10.07	88.46	16.89
11	Vm	S	0.5	0.59	8.39	0.07	8.17	84.41	19.92
12	Vm	L	1.5	0.62	8.20	0.09	12.39	83.88	19.57
13	VmC	NA	6	0.50	8.09	0.07	9.01	79.15	21.36
14	VmC	SS	3.5	0.60	8.33	0.12	9.14	101.10	16.43
15	VmC	S	1.5	0.60	9.22	0.17	7.43	79.36	23.24
16	VmC	L	0.5	0.59	7.43	0.09	9.01	79.99	18.04

### 3.2.1 Fibre orientation distribution ( $\alpha$ )

The contribution percentages in ANOVA and the S/N ratio indicated that the fibre aspect ratio ( $Ar$ ) was the primary affecting parameter for the fibre orientation distribution. As the fibre length increases, the direction of glass fibre in the mixture moves further away from a 3-D random condition and tends to approach a 2-D aligned situation due to the influence of the wall. This effect was even more apparent in the case of L-type rGFs, whose average fibre length was close to or exceeded the width of the mould. During the pouring process, the boundaries restricted the random orientation of the fibres, forcing fibres (especially near the edge) to align longitudinally.

The production method ( $P_m$ ) was the second significant factor affecting fibre orientation. Samples produced by vibration ( $Vib$ ) had the highest average fibre orientation factor values compared to the other three methods. It is worth noting that the vibration period was 5 mins in the current study. Since the impregnated glass fibre is much lighter than the IP paste when the fibre IP mixture vibrates, the fibres tend to float up and reorientate horizontally during the vibration process. In the current case, the fibre content ( $F_n$ ) seems to be a negligible factor was probably due to the sufficient mixing time (5 mins) and the good workability of the fresh IP mixture, which allowed rGF to be dispersed in the paste well.

### 3.2.2 Porosity and pore distribution ( $P$ )

MIP showed that most pore volumes were related to micropores and capillaries for pure IP samples. These originated from the mixing operations between the solid components of the hydrated slurry, with only 0.2%-0.5% porosity by volume above 15  $\mu\text{m}$ , regardless of the production method. Figure 3(b) shows that all selected parameters significantly affected the total porosity ( $P$ ). Both S/N ratio and ANOVA showed that the fibre length ( $Ar$ ) was marginally the most influential factor for  $P$ . This is because long fibres tend to get inhomogeneously dispersed and form agglomerates, leading to excessive void formation due to poor compaction. The results also pointed out that S-type rGFs introduced more porosity than L-type rGFs. The S-type has a rougher surface with curling and branching and can be easily agglomerated, resulting in significantly more pores entrapped between fibre bundles. Surprisingly, in terms of exploring production methods ( $P_m$ ) to reduce porosity, the average porosity value indicated vibration as ineffective for removing micropores and capillaries. As shown in Figure 3(c) and Figure 4,  $P_m$  was found to significantly alter the number of large macro voids trapped in the matrix. The current study observed an approximately 74% decrease in air content by vacuum mixing (lowering the pressure from 1014 to 100 mbar). Studies on concrete in the open literature confirmed that mixing the concrete under a reduced air pressure decreases the macro voids [9]. Using a cartridge to place the paste after vacuum mixing can further eliminate the large visible pores, which is attributed to the breakage of air bubbles in the IP touching the cartridge walls under the effects of the squeezing motion.

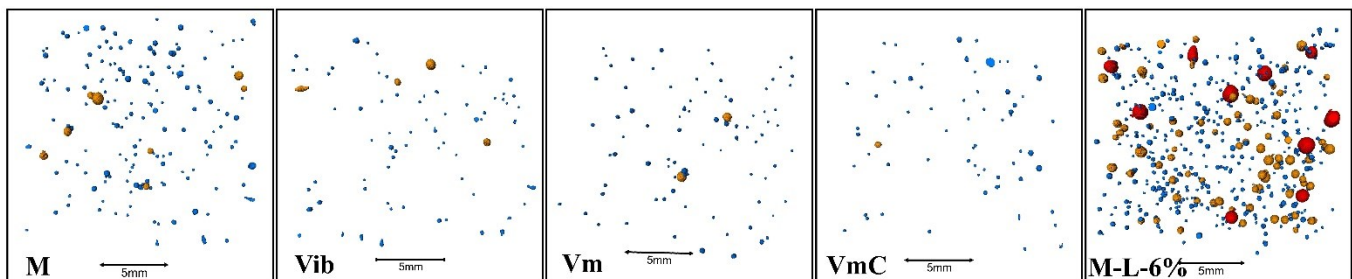


Figure 4. Macro pore visualization reconstruction CT images of IPs produced by: mixing (M), vibrating mixing (Vib), Vacuum mixing (Vm), vacuum mixing and cartridge (VmC) and addition of L-rGFs (M-L-6%). Pores are labelled in colours based on their diameter range: >1mm is red, between 1mm and 0.5mm is yellow; ranging between 0.5mm and 200 $\mu\text{m}$  is blue.

### 3.2.3 Flexural and compressive strength ( $F_s$ , $C_s$ )

Figure 3 (d) and (e) depict the effects of selected parameters on means of  $F_s$  and  $C_s$ . Trends of the influence of selected parameters showed a big difference in the composite's flexural and compressive strength. It can be seen that  $F_s$  increased with rises in fibre length and fibre content. Pure IP pastes typically fail in opening mode, and the addition of fibre can overcome such failure by providing a higher resistance to crack formation and expansion. The rGFs used in this study, such as S- and L-types, were usually bifurcated fibre bundles and partially covered by resin residues. The ruggedness and roughness increase the mechanical interlocking and friction resistance between the fibres and IP concrete. A larger fibre aspect ratio ensures effective stress transfer over a larger section of fibre, while increasing the fibre content generally leads to enhanced composite strength, e.g., an enhanced fibre bridging effect. In the present study, an increase in  $F_s$  was observed when the fibre aspect ratio increased to the maximum level of 25 and the fibre content ranged from 0.5 to 6 vol%. Even though adding a high content of long fibres introduced pores and heterogeneity, the fibre-IP binder interaction was sufficient to overcome the weakness due to the porous structure in the abovementioned fibre length/content range. This follows the laws of composites mechanics and is confirmed by the literature, where the flexural strength of composites increases when the fibre content is increased to values less than 8 vol%, regardless of the fibre type [14].

However,  $C_s$  demonstrated more irregular trends with the increase in fibre length and fibre content, as observed in the literature [15]. Compression strength at the fibre levels used is dominated by the matrix (IP) strength and for the rest strongly depends on the fibre/matrix interaction, strength and dispersion of the fibres and defects present in the material. Above a fibre content of 3.5%, adverse effects of fibres appeared, which led to a significant increase in porosity and poor fibre dispersion. This effect was more severe in multifilament (e.g. type S and L rGFs) than in single fibres (type SS). Compression strength increased significantly upon introduction of the fibres, but at higher Ar apparently, the more slender fibres buckled more easily, leading to a decrease in  $C_s$ .

The S/N ratio and ANOVA results agreed: fibre aspect ratio (Ar) was the most significant factor affecting the flexural strength ( $F_s$ ), whereas producing method (Pm) contributed most to compressive strength ( $C_s$ ). Although Pm showed a minor contribution to  $F_s$ , its low P-value (<0.1) indicates importance. Furthermore, opposite effects of Pm were observed on  $F_s$  and  $C_s$ : from regular mixing to combo methods, such as Vib, Vm and VmC,  $F_s$  strongly decreased whereas  $C_s$  increased significantly, which was due to their different sensitivities to the local and overall properties of the material.

### 3.2.4 Young's modulus ( $E_s$ )

As shown in Figure 3(f), the elastic modulus at the initial uncracked stage ( $E_s$ ) was predominately governed by Pm. In contrast, the ultimate horizontal strain for the multi-cracking phase was highly dependent on the Ar. The measured flexural stress-strain curves showed quite different behaviour for the various reinforced IP materials (Figure 5): unreinforced IP showed a brittle character with abrupt fracture of the specimen, while rGFs-IP showed a more elastoplastic behaviour. The first stage represented a linear elastic segment with a steep slope, which represents the uncracked response of the sample. This was similar for all samples tested since apparently, in this stage, the behaviour of the prism was mainly dominated by the unreinforced IP material with an E-modulus of around 18 GPa, and the amount of added reinforcement was apparently too small to have an apparent effect; please note that glass fibre reinforced epoxy rods would have an E-modulus of approximately 35 GPa and only a few percent of these were added to the IP. As the applied load increased, the reinforced materials did not fatally crack but showed a remarkably ductile behaviour due to crack bridging by the fibres, leading to remarkably higher strength and strain-to-failure values than the unreinforced material. As the specimen underwent multiple cracking stages, only fibres bore the load until failure due to rupture or sliding, resulting in the formation of multiple

microcracks instead of several large cracks. As a result, the ductility of the material increased. This explains the observation in Section 3.2.3 that fibre-related characteristics ( $A_r$ ,  $F_n$ ) determined  $F_s$ . In a similar fashion, longer fibres ( $A_r$ ) and a higher content of fibres ( $F_n$ ) will all benefit crack bridging and lead to a higher strain to failure.

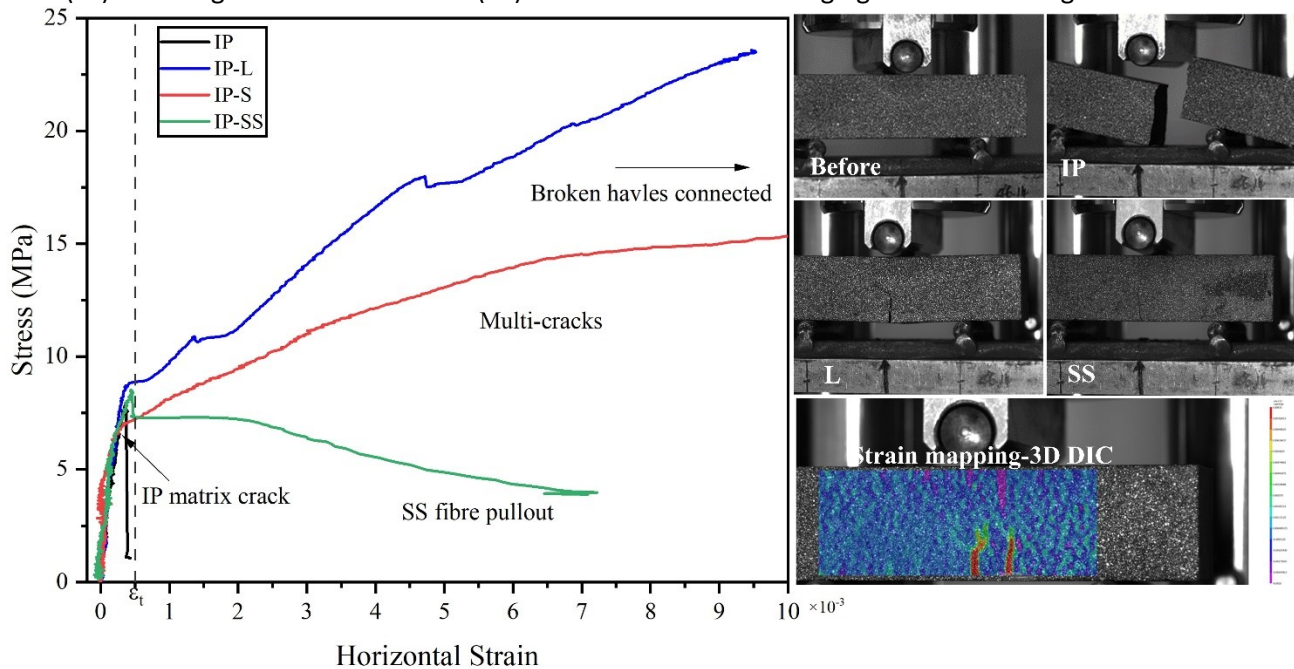


Figure 5. Typical stress-strain curves and fracture patterns for specimens.

### 3.3 Selection of optimum parameters and their effectiveness

Using the Taguchi method, it was found that the predicted optimum parameters to obtain a high compressive strength (expected value was 93 MPa) was the addition of 3.5 vol% of super short rGFs to the IP and the use of vacuum mixing to mix and a cartridge to place the mixture (SS-3.5%-VmC). The best parameters to obtain high flexural strength (predicted value was 24 MPa) was the addition of 6 vol% of long rGFs and vibratory placement of the mixture (Vib-L-6%). For validating the Taguchi predicted optimum conditions, confirmation tests were conducted. The measured compressive strength for the SS-3.5%-VmC sample reached 101 MPa (std. 6.7MPa,  $F_s$  9.1MPa) and the flexural strength for Vib-L-6% amounted to 28 MPa (std. 1.1 MPa,  $C_s$  84.1MPa) at 7 days of curing. Outcomes of the current optimized recycling route for GFRP waste-reinforced Fe-rich inorganic polymers are promising: the flexural strength enhancement compared to the state-of-the-art stands out, reaching a gain of 215%; the improvement in compressive strength is at a moderate level of about 32%. The absolute strength exceeds the reported properties of fibre-reinforced cementitious materials, of which the flexural strength and compressive strength range from 3 to 12 MPa and from 20 to 70 MPa, respectively [4,8,15–17].

## 4 CONCLUSIONS

To improve the recycling efficiency and explore the new end-application possibilities of the GFRP recyclates with high-performance gains, this research group proposes a promising recycling route where roller milling recycled GFRP waste, including resin residues, are used as reinforcement for iron-rich inorganic polymers produced from non-ferrous metallurgical residues, which has only recently been evaluated for valorization in building materials. The proposed recycling route was optimized by a sensitivity factor analysis.

It is found that roller milling produced more concentrated elongated glass fibre recyclates than disc milling; its content depended on the setting parameters of the roll gap and mixing time. Fibre orientation and distribution in the matrix were mainly influenced by the fibre aspect ratio (Ar) due to the mould wall effect. The porosity of the matrix was most affected by Ar and producing method (Pm). The processing steps, such as vibrating (Vib), vacuum mixing (Vm) and cartridge (VmC), considerably reduced the number of large voids trapped in the matrix. Compression and initial elastic modulus were mainly affected by choice of the Pm, followed by the Ar; they greatly modified the macropore structure and fibre dispersion in the matrix. Flexural strength and post-cracking behaviour were highly dependent on the fibre-related parameters- Ar, followed by fibre content (Fn), and lastly Pm. The measured compressive strength for the optimized product- SS-3.5%-VmC sample- reached 101 MPa (std. 6.7MPa, Fs 9.1MPa) and the flexural strength for Vib-L-6% amounted to 28 MPa (std. 1.1 MPa, Cs 84.1MPa) at 7 days of curing. The flexural strength enhancement compared to the state-of-the-art stands out, reaching a gain of 215%; the compressive improvement is at a moderate level of 32%.

## 5 REFERENCES

- [1] Shuaib NA, Mativenga PT. "Energy demand in mechanical recycling of glass fibre reinforced thermoset plastic composites". *Journal of Cleaner Production* 2016;120:198–206.
- [2] Pickering SJ. "Recycling technologies for thermoset composite materials—current status". *Composites Part A: Applied Science and Manufacturing* 2006;37(8):1206–15.
- [3] Stella Job. "Recycling glass fibre reinforced composites: history and progress". *Reinforced Plastics* 2013;57(5):19–23.
- [4] Zhang Y, Pontikes Y, Lessard L, van Vuure A. "Recycling and valorization of glass fibre thermoset composite waste by cold incorporation into a sustainable inorganic polymer matrix". *Composites Part B: Engineering* 2021;223:109120.
- [5] van de Sande J, Peys A, Hertel T, Rahier H, Pontikes Y. "Upcycling of non-ferrous metallurgy slags: Identifying the most reactive slag for inorganic polymer construction materials". *Resources, Conservation and Recycling* 2020;154:104627.
- [6] Ascensão G, Beersaerts G, Marchi M, Segata M, Faleschini F, Pontikes Y. "Shrinkage and Mitigation Strategies to Improve the Dimensional Stability of CaO-FeOx-Al<sub>2</sub>O<sub>3</sub>-SiO<sub>2</sub> Inorganic Polymers". *Materials (Basel)* 2019;12(22).
- [7] Peys A. "Inorganic polymers from CaO-FeO-SiO<sub>2</sub> slags: Processing, reaction mechanism and molecular structure", Graduate Theses and Dissertations KU Leuven; 2018.
- [8] Coppola L, Cadoni E, Forni D, Buoso A. "Mechanical Characterization of Cement Composites Reinforced with Fiberglass, Carbon Nanotubes or Glass Reinforced Plastic (GRP) at High Strain Rates". *AMM* 2011;82:190–5.
- [9] Dils J, Boel V, Schutter G de. "Vacuum mixing technology to improve the mechanical properties of ultra-high performance concrete". *Mater Struct* 2015;48(11):3485–501.
- [10] Sivaiah P, Chakradhar D. "Modeling and optimization of sustainable manufacturing process in machining of 17-4 PH stainless steel". *Measurement* 2019;134:142–52.
- [11] Parviz Soroushian and Cha-Don Lee. "Distribution and Orientation of Fibers in Steel Fiber Reinforced Concrete". *MJ* 1990;87(5).
- [12] Dupont D, Vandewalle L. "Distribution of steel fibres in rectangular sections". *Cement and Concrete Composites* 2005;27(3):391–8.
- [13] EN 196-1:2005. "Methods of testing cement - Part 1: Determination of strength". Brussels: EUROPEAN STANDARD; 2005.
- [14] Ranjbar N, Talebian S, Mehrali M, Kuenzel C, Cornelis Metselaar HS, Jumaat MZ. "Mechanisms of interfacial bond in steel and polypropylene fiber reinforced geopolymer composites". *Composites Science and Technology* 2016;122:73–81.
- [15] Alomayri T, Low IM. "Synthesis and characterization of mechanical properties in cotton fiber-reinforced geopolymer composites". *Journal of Asian Ceramic Societies* 2013;1(1):30–4.
- [16] Novais RM, Carvalheiras J, Capela MN, Seabra MP, Pullar RC, Labrincha JA. "Incorporation of glass fibre fabrics waste into geopolymer matrices: An eco-friendly solution for off-cuts coming from wind turbine blade production". *Construction and Building Materials* 2018;187:876–83.
- [17] Fox TR. "Recycling wind turbine blade composite material as aggregate in concrete". Graduate Theses and Dissertations, Iowa State University; 2016.